Calibration Method for Fully Polarimetric Microwave Radiometers Using the Correlated Noise Calibration Standard

Jinzheng Peng, *Member, IEEE*, and Christopher S. Ruf, *Fellow, IEEE*

***Abstract*—In this paper, a new and improved L-band version of the correlated noise calibration standard (CNCS) has been developed to aid in the characterization of polarimetric microwave radiometers. The CNCS generates a series of known polarimetric test signals using a two-channel commercial arbitrary waveform generator (AWG) and a pair of frequency-upconversion modules. When it is inserted in place of the antenna used by a radiometer-under-test (RUT), it can fully characterize the polarimetric response of the receiver portion of the RUT. Both hardware and software improvements have been made over a previous version of the CNCS. The frequency upconverters now include integral warm and cold calibration-reference targets to automatically compensate for small drifts in AWG output-signal strength. The procedure used to calibrate the RUT has been generalized to correct for nonideal characteristics of the CNCS itself. Moreover, the effects on the derived polarimetric gain matrix of impedance mismatches between the RUT, and either the CNCS or the antenna have been determined. Details of the CNCS improvements are presented. The results of an experimental demonstration of its use and of a series of validation tests of its performance are also presented.**

***Index Terms*—Calibration, microwave radiometry, noise generators, polarimetry.**

I. Introduction

A POLARIMETRIC radiometer measures the strength and polarization state of thermally radiated electric fields, as described under the Rayleigh–Jeans approximation by the modified Stokes parameters in brightness temperature [1]–[3]. Measurements can be made either coherently, by directly correlating orthogonal components of the electric field, or incoherently, by considering differences between slant linear and circularly polarized brightness temperatures [4]–[7].

Calibration of a polarimetric radiometer is possible using a signal generator that can create controllable and repeatable partial correlation between vertically and horizontally polarized (v- and h-pol) signals. Several such calibrators have been developed. A system capable of coupling three predetermined test signals into the antenna feed of a millimeter-wave radiometer has been developed [8]. A polarized blackbody load has been developed to produce partial in-phase correlated calibration signals by varying the relative alignment between the load and the radiometer's antenna [9]. This technique has been expanded to include the generation of partial quadrature-phase correlation using a phase-retardation plate [10]. A third method, the correlated noise calibration standard (CNCS), uses a programmable digital noise source to generate partially correlated signals at power levels similar to those delivered by an actual radiometer antenna [11]. The CNCS is typically installed in place of the antenna and, so, can be used to characterize and calibrate a radiometer's receiver. However, it would not provide a complete end-to-end calibration of the radiometer including its antenna. The CNCS is capable of producing a wide range of test signals that can be used to characterize the receiver. Signals can be generated with independently controlled levels of first, second, third, and fourth Stokes brightness temperatures.

An X-band version of the CNCS has been used previously to characterize the correlating receivers in the NASA/U-Michigan airborne Lightweight Rainfall Radiometer [12]. A new and improved L-band version has recently been completed. It is being used to evaluate the performance of the polarimetric radiometer on Aquarius (a low Earth-orbiting ocean-salinity mission) [13], [14]. The third Stokes channel in the Aquarius radiometer is used to estimate the degree of ionospheric Faraday rotation [3]. Since there is no fourth Stokes channel, it is important to measure the phase imbalance between v- and h-pol channels in order to characterize the radiometer's susceptibility to the fourth Stokes parameter, which may be significant and may vary as a function of surface wind speed [15]. In addition, the stability of the Aquarius radiometer calibration on time scales of days is particularly relevant [13].

In order to calibrate a radiometer-under-test (RUT) using the CNCS, the CNCS itself also needs to be characterized. A parameterized forward model has been developed which describes its characteristics, including nonideal properties, and an associated inversion algorithm has been developed that simultaneously characterizes the CNCS and calibrates the RUT.

In this paper, the CNCS and a benchtop correlating polarimetric radiometer are described in Section II. Section III presents the calibration algorithm, which consists of parameterized CNCS and RUT forward models. Detailed descriptions of the test procedures followed to generate the measurements needed to perform an inversion of the forward models and of the data analysis used to solve for the unknown parameters of the models are given in a series of Appendices. Section IV presents the results of the calibration and also describes a number of tests that were conducted to verify the validity of the results.

Manuscript received September 24, 2007; revised January 2, 2008 and February 18, 2008. Current version published October 1, 2008. This work was supported in part by the National Aeronautics and Space Administration under Research Grant NNZ04HZ28C and Contract NNG05CA07C.

The authors are with the Space Physics Research Laboratory, University of Michigan, Ann Arbor, MI 48109 USA.

Color versions of one or more of the figures in this paper are available online at http://ieeexplore.ieee.org.

Digital Object Identifier 10.1109/TGRS.2008.2000740

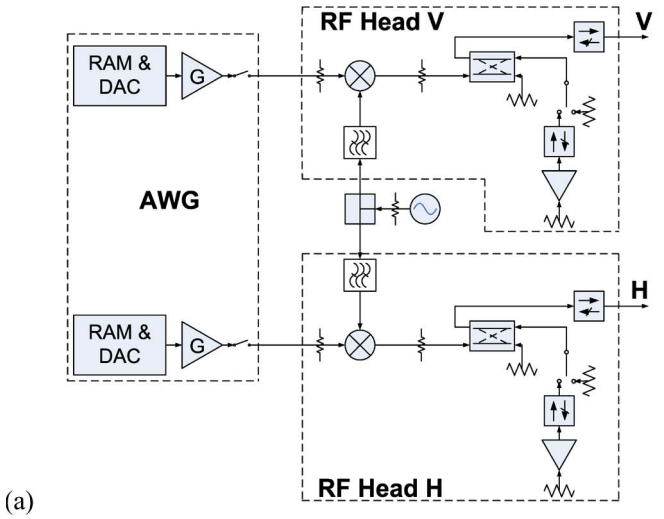

(a)

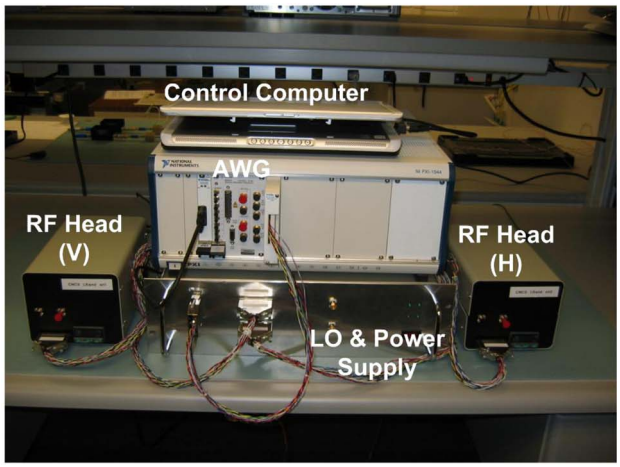

(b)

Fig. 1. (a) Functional block diagram and (b) photo of the L-band CNCS.

II. Hardware Description

A. CNCS—A Programmable Digital Noise Source

A functional block diagram of the CNCS and a photo are shown in Fig. 1. The system consists of a commercial arbitrary waveform generator (AWG), a pair of frequency-upconversion modulators with integral calibration-reference sources (referred to as the "RF Heads"), and a local oscillator (LO) which provides coherent LO signals for the two channels through a power divider.

The AWG is an Agilent model N6030A with fixed 1.25-GS/s internal sample clock. It has two independent output channels with maximum analog bandwidths of 500 MHz. The correlation between the pair of signals is determined by the values loaded into the lookup tables of the AWG [11]. The values are converted into analog signals by a pair of 15-bit digital-to-analog converters (DACs) that are synchronously triggered by the internal sample clock. The strength of the analog signals exiting the DACs are adjusted by amplifiers with 3.3 dB of gain control. AWG output signals can also be commanded on and off.

The AWG signals are upconverted by RF Heads to the operating frequency of the RUT. The RF Heads include an ambient blackbody load and an active cold load to correct for variations in AWG output power. They are housed in a thermally controlled environment with a typical temperature stability of 0.05 °C rms over time scales of tens of minutes. The temperatures of the ambient and cold loads are continuously monitored to allow for temperature-dependent corrections to their brightness temperatures. The active cold load, which is a backward-installed low noise amplifier (LNA), provides an uncorrelated noise background for the output signal of each channel. To increase the electrical isolation between parts, isolators and attenuators are inserted in several places, as shown in Fig. 1. A bandpass filter is also used in each RF Head to reduce unwanted RF and IF signal leakage between channels. This eliminates any significant crosstalk between the v- and h-pol channels and ensures that the degree of partial correlation between channels is due solely to the AWG programming.

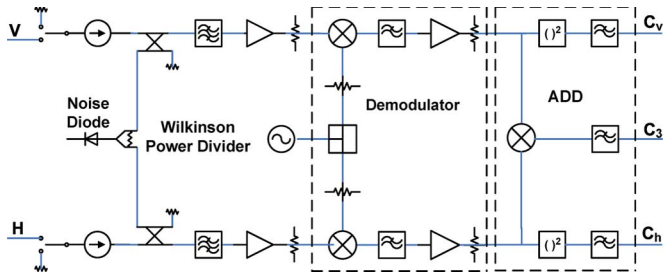

Fig. 2. System block diagram of the L-band polarimetric RUT. The in-phase, but not the quadrature-phase, part of the correlation between v- and h-pol signals is computed, resulting in a measurement capability for T_v, T_h, and T_3 but not T_4.

B. L-band Correlating Polarimetric Radiometer

A benchtop L-band radiometer, built by the Space Physics Research Laboratory of the University of Michigan, was used to demonstrate and validate the calibration methodology of the CNCS. Its system block diagram is shown in Fig. 2. Input v- and h-pol signals are filtered and amplified, then coherently down-converted to an IF band. The IF signals are then processed by the Agile Digital Detector (ADD) [16]. ADD digitizes the input signals and implements digital-signal-processing operations to measure the Stokes parameters. The first and second Stokes parameters are measured by the self-correlation of the two individual input signals, while the third Stokes parameter is measured by their cross-product. Matched loads connected to the input switches, together with a noise diode, are used for intermittent calibration, with the radiometer operated, otherwise, in total power mode. The noise-diode signal is divided by a Wilkinson power divider and coupled into the two radiometer channels.

III. Hardware Forward Model to be Calibrated

A. CNCS Forward Model

A parameterized forward model for radiative transfer through the CNCS is used to represent the relationship between its user-controlled settings and the signals that it injects into the RUT. The strength of the signal generated by the AWG is controlled in two ways. The relative signal level over time is determined by the numerical values that are loaded into its software lookup

table. The lookup table defines a normalized version of the signal. The absolute signal strength is determined by an AWG voltage gain setting G. The gain setting can be varied in software from 0.17 to 0.25. This amounts to a variation in the AWG output power of 3.3 dB. Variations in the AWG output power have been verified, using a high-precision power meter, to be linearly related to G^2 to better than 99.986%.

Signals generated by the CNCS contain one component generated by the AWG and a second component originating from either an ambient matched load or an active cold load. The brightness temperature of the AWG signal, referenced to the output of the RF Head, can be expressed as

$$T_{\mathrm{awg}} = k(G^2 T_n + O_{\mathrm{awg}}) \tag{1}$$

where k is a scale factor used to represent gain imbalance between the two CNCS channels, $T_n = 4480$ K is the nominal brightness temperature generated by the AWG as defined by the lookup table, and O_{awg} is a possible offset brightness temperature.

The total brightness temperature of each individual CNCS channel is the sum of the AWG component plus that of either the ambient load or active cold load. If the two CNCS channels are used as inputs to the vertical and horizontal polarization channels of a fully polarimetric radiometer, then the quadrature components of correlation between them will represent the third and fourth Stokes parameters. Decorrelation between the two CNCS channels due to differences in the phase of the transfer functions is assumed to be negligible when used to calibrate the L-band RUTs considered in this paper, because the radiometers' RF bandwidths are considerably narrower than that of the signal path through the RF Heads of the CNCS. It should be noted that this simplifying assumption might not be the case when calibrating a radiometer with a much wider bandwidth.

The complete CNCS forward model is given by

$$\begin{aligned}
T_v &= k_v\left(G_v^2 T_n + O_{\mathrm{awg},v}\right) + T_{y,v} \\
T_h &= k_h\left(G_h^2 T_n + O_{\mathrm{awg},h}\right) + T_{y,h} \\
T_3 &= 2 \cdot \sqrt{k_v(G_v^2 T_n + O_{\mathrm{awg},v}) \cdot k_h(G_h^2 T_n + O_{\mathrm{awg},h})} \\
&\quad \cdot \rho \cos(\theta + \Delta) \\
T_4 &= 2 \cdot \sqrt{k_v(G_v^2 T_n + O_{\mathrm{awg},v}) \cdot k_h(G_h^2 T_n + O_{\mathrm{awg},h})} \\
&\quad \cdot \rho \sin(\theta + \Delta)
\end{aligned} \tag{2}$$

where k_v and k_h may differ in accounting for possible gain imbalances between the vertical and horizontal channels, G_v and G_h are the voltage gains of the respective AWG channels, $O_{\mathrm{awg},v}$ and $O_{\mathrm{awg},h}$ are the offsets of the AWG channels, ρ and θ are the magnitude and phase of the correlation coefficient between the two channels, Δ is the electrical-path-length imbalance between the two CNCS channels (resulting in a phase offset in the correlation, where a positive value for Δ means that the electrical path length of the h-pol channel is longer than that of the v-pol channel), and $y =$ ambient or cold designates the background reference load selected in the RF Head. User-determined parameters of the CNCS forward model include the AWG gain settings (G_v, G_h), and the complex correlation coefficient (ρ, θ). The nonideal parameters of the forward model, which need to be determined as part of the calibration procedure, are the gain imbalances (k_v, k_h), the AWG channel offsets $(O_{\mathrm{awg},v}, O_{\mathrm{awg},h})$, and the interchannel phase imbalance Δ.

B. Polarimetric-Radiometer Forward Model

Calibration of a radiometer consists of determining each parameter in its forward model. What forward model to use depends on the particular radiometer type. Examples of forward models appropriate for several coherent- and incoherent-detection radiometer architectures are considered here for illustrative purposes.

For a fully polarimetric radiometer that uses incoherent detection, the forward model is given by

$$\begin{pmatrix} C_v \\ C_h \\ C_p \\ C_m \\ C_l \\ C_r \end{pmatrix} = \begin{pmatrix} G_{vv} & G_{vh} & G_{v3} & G_{v4} \\ G_{hv} & G_{hh} & G_{h3} & G_{h4} \\ G_{pv} & G_{ph} & G_{p3} & G_{p4} \\ G_{mv} & G_{mh} & G_{m3} & G_{m4} \\ G_{lv} & G_{lh} & G_{l3} & G_{l4} \\ G_{rv} & G_{rh} & G_{r3} & G_{r4} \end{pmatrix} \cdot \begin{pmatrix} T_v \\ T_h \\ T_3 \\ T_4 \end{pmatrix} + \begin{pmatrix} O_v \\ O_h \\ O_p \\ O_m \\ O_l \\ O_r \end{pmatrix} \tag{3}$$

where C_x for $x = v, h, p, m, l,$ and r are the raw radiometer measurement "counts" for each of its six polarimetric channels, T_y for $y = v, h, 3,$ and 4 are the input Stokes parameters, G_{xy} are the gain matrix elements that relate input signals to output measurements, and O_x are offsets in the measurements that are not related to the input signals. The 30 unknown parameters that need to be determined in this forward model are the G_{xy} and O_x. For the Aquarius radiometer, since there are no left- and right-hand circular polarization channels, the appropriate forward model is a simplified version of (3) that omits C_x, O_x, and G_{xy} for $x = l$ and r and $y = v, h, p, m, l,$ and r. In this case, there would only be 20 unknown parameters to be determined. Note that the input signal T_4 cannot be omitted, since it can still influence the measurements if there is any polarization leakage present.

The forward model for a fully polarimetric radiometer that uses coherent detection is given by [20]

$$\begin{pmatrix} C_v \\ C_h \\ C_3 \\ C_4 \end{pmatrix} = \begin{pmatrix} G_{vv} & G_{vh} & G_{v3} & G_{v4} \\ G_{hv} & G_{hh} & G_{h3} & G_{h4} \\ G_{3v} & G_{3h} & G_{33} & G_{34} \\ G_{4v} & G_{4h} & G_{43} & G_{44} \end{pmatrix} \cdot \begin{pmatrix} T_v \\ T_h \\ T_3 \\ T_4 \end{pmatrix} + \begin{pmatrix} O_v \\ O_h \\ O_3 \\ O_4 \end{pmatrix}. \tag{4}$$

There are 20 unknown parameters (G_{xy} and O_x) to be determined in this case. If the radiometer uses coherent detection without a fourth Stokes channel (i.e., measures only the in-phase component of the correlation between v- and h-pol signals), then the forward model will be a simplified version of (4) in which C_4, G_{4y}, and O_4 for $y = v, h, 3,$ and 4 are omitted. In this case, there would be 16 unknown parameters to be determined. This last case applies to the benchtop radiometer that has been used to experimentally validate the performance of the new L-band CNCS, the results of which are presented in Section IV as follows.

TABLE I
CNCS-CALIBRATION TEST SET

Test Vector	ρ	Θ	G_v	G_h	AWG signal	v- and h-pol Background TB
t_1	0	0	0.17	0.17	On	Cold
t_2	0	0	0.17	0.17	Off	Cold
t_3	0	0	0.17	0.17	Off	Ambient
t_4	0	0	0.25	0.17	On	cold
t_5	0	0	0.25	0.17	Off	cold
t_6	0	0	0.25	0.17	Off	ambient
t_7	0	0	0.17	0.25	On	cold
t_8	0	0	0.17	0.25	Off	cold
t_9	0	0	0.17	0.25	Off	ambient
t_{10}	1	0	0.25	0.25	On	cold
t_{11}	1	0	0.25	0.25	Off	cold
t_{12}	1	0	0.25	0.25	Off	ambient
t_{13}	1	45°	0.25	0.25	On	cold
t_{14}	1	45°	0.25	0.25	Off	cold
t_{15}	1	45°	0.25	0.25	Off	ambient

C. Inversion of the Instrument Forward Model

The forward models for both the CNCS and radiometer can be combined together into a single composite forward model, which relates the desired brightness temperatures that are programmed into the CNCS to the output digital counts that are measured by the RUT. In order to simultaneously retrieve both the gain matrix and offsets of the radiometer together with the CNCS forward-model parameters, a suitable set of test data is required. The test data are generated by varying CNCS software settings [ρ, θ, G_v, and G_h in (2)] and hardware switch positions (AWG signal either on or off; background TB source either ambient or cold load). The complete combination of CNCS settings that was used for the results presented here is listed in Table I. There is some redundancy of information provided by this set of test vectors. However, the precision and reliability of the retrieved forward-model parameters is improved by over constraining the system of equations from which they are derived; therefore, the redundancy is retained.

All elements of the radiometer gain matrix and measurement offset, and all parameters of the CNCS forward model except for its channel phase imbalance Δ, can be satisfactorily estimated from the measurements using an over constrained nonlinear iterative minimization method. The dependence of the channel phase imbalance on the test settings is not sufficiently unique, relative to the other parameters, to be retrievable by inversion of the complete forward model, given a calibration data set that can be generated automatically (many of the characterization tests that are enabled by the CNCS become extremely laborious if the calibration test set is not automatically generated). The CNCS channel phase imbalance must be estimated by manually cross-swapping the interconnecting cables between the CNCS and the RUT. This is the one step in the calibration procedure that is not fully automated. Fortunately, the channel phase imbalance has, in practice, been found to be extremely stable over time and, so, not in need of frequent recalibration.

The complete set of unknown parameters in the composite forward model for both the CNCS and RUT can be combined together into a single unknown vector $\overline{X}$, given by

$$\overline{X} = \{k_v, k_h, O_{\mathrm{awg},v}, O_{\mathrm{awg},h}, \Delta, G_{mn}, \text{and } O_m\} \tag{5}$$

where $m = v, h, p, m, l,$ and r for a fully polarimetric incoherent-detection radiometer, $m = v, h, 3,$ and 4 for a fully polarimetric coherent-detection radiometer, and $n = v, h, 3,$ and 4 in either case. The individual elements of $\overline{X}$ are defined in (2), (3), and (4). All of the radiometer measurements made during the calibration test can be similarly combined into a measurements vector $\overline{C}$, given by

$$\overline{C} = f(\overline{X}) \tag{6}$$

where each element of $\overline{C}$ is the measurement count for one of the six polarimetric-radiometer channels at one of the 15 CNCS settings listed in Table I and f represents the composite forward model.

The estimation of $\overline{X}$ given $\overline{C}$ is performed by inverting (6) using the iterative Newton–Raphson method. Specifically, a first guess at $\overline{X}$ is made, denoted by $\hat{\overline{X}}$. The Jacobian matrix J of partial derivatives of f with respect to elements of $\overline{X}$, evaluated at $\hat{\overline{X}}$, is next computed numerically. An updated estimate of $\hat{\overline{X}}$ is then made according to

$$\hat{\overline{X}}' = \hat{\overline{X}} + (J^T \cdot J)^{-1} \cdot J^T \cdot \left(\overline{C} - f(\hat{\overline{X}})\right). \tag{7}$$

This process is iterated until changes in $\hat{\overline{X}}$ become vanishingly small, and $\hat{\overline{X}}$ has converged to that value which minimizes the norm-squared difference between $\overline{C}$ and $f(\hat{\overline{X}})$. Determining the parameters of the RUT forward model is equivalent to calibrating it.

One other correction to the RUT forward model is necessary if the impedance match between it and the CNCS differs from the match with the antenna that would be connected in place of the CNCS during normal data taking. The impedance mismatch between the CNCS and RUT receiver has two potential effects—it can change the apparent brightness temperature of the CNCS active cold load and it can alter a number of the elements of the RUT's polarimetric gain matrix and offset vector, relative to what they would be when connected to an antenna with a different impedance match. Corrections for both of these effects are considered here. The impact of impedance mismatches between a radiometer receiver and its antenna on the digital counts measured by the radiometer has been addressed previously by Corbella *et al.* [17], [18]. Their approach

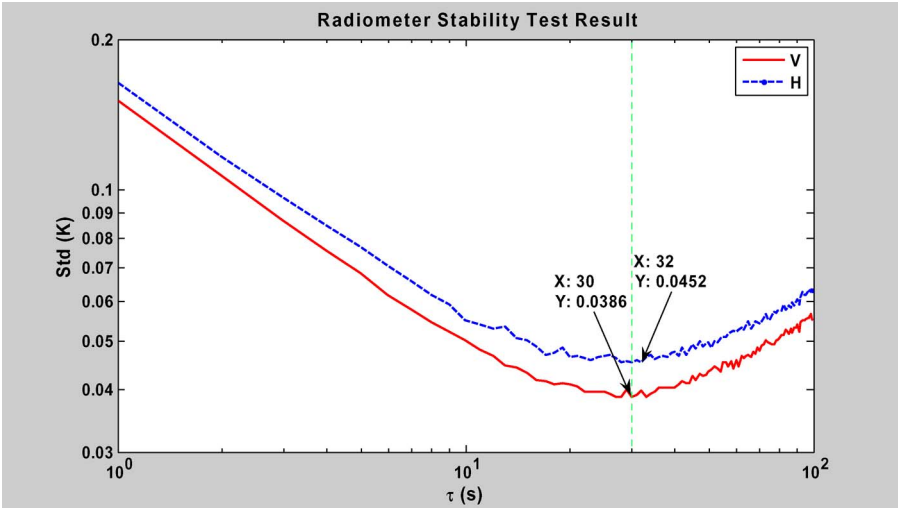

Fig. 3. Allan standard deviation versus integration time of free-running radiometer characterizes the inherent stability of the radiometer receiver.

is adopted here, generalizing the input-impedance mismatch to include that with the CNCS as well as the antenna. In summary, the apparent brightness temperature of the CNCS active cold loads increases by 2.1 and 2.3 K for the v- and h-pol channels, respectively, due to the reflection of a small fraction of the RUT receiver noise temperature at the mismatched cold-load interface. As a result of the high (∼75 dB) isolation between v- and h-pol channels of the CNCS, elements of the RUT gain matrix require only insignificantly small corrections. However, the offset brightness temperatures, O_v and O_h in (3) and (4), do require small but significant corrections. A detailed derivation of the corrections to the forward-model parameters due to impedance mismatches is provided in the Appendix.

IV. Data-Taking Procedures and Results of Calibration With the CNCS

The test procedures that were followed to calibrate the bench-top RUT with the CNCS, together with the resulting estimates of the parameters of the CNCS and RUT forward models and of their accuracy and precision, are described in this section.

A. Radiometer Stability

The calibration test set consists of 15 variations of the input signals generated by the CNCS (see Table I). During the time over which the test set is generated, both the CNCS and radiometer forward models should not vary appreciably. The stability of the radiometer is determined from a long time series of measurements made while continuously observing the CNCS reference load (i.e., calibration test signal t_3 in Table I) in its "total power" mode—without any calibration of radiometer-gain variations or any correction for the very small variations in the physical temperature of the reference load. The Allan variance of the measurements is used to characterize the stability of the radiometer [19]. Fig. 3 shows the derived Allan standard deviation of the radiometer measurements versus integration time for both the v- and h-pol channels. The minimum standard deviation occurs at an integration time of 30 and 32 s for the v- and h-pol channels, respectively. Based on these results, a complete calibration data set should be completed in no more than 30 s. The results presented here are based on measurements made with a dwell time of 2 s on each of the 15 calibration-test settings.

B. CNCS Stability

CNCS stability is characterized by using a similar Allan-variance analysis but with the radiometer observing a CNCS signal composed of an active-cold-load background to which an AWG signal is added that raises the brightness temperature to that of the ambient load. This choice is made under the assumption that the dominant source of drifting in the CNCS signal will be the stability of the AWG output-signal strength. In order to remove the effects of drifts in radiometer gain, data are taken in a repeated cycle of the CNCS ambient load, cold load alone, and AWG + cold load (i.e., calibration test signals t_1, t_2, and t_3 in Table I). Dwell time on each of these signals is 5 s. Adjacent ambient and cold-load measurements are used to calibrate the radiometer for each AWG + cold-load measurement in order to remove the effects of radiometer drift. Fig. 4 shows the resulting Allan standard deviation of the calibrated AWG + cold-load time series versus elapsed time. The available integration time for the AWG + cold load is one third of the elapsed time because of the 33% dwell time on each of the three signals. The minimum standard deviations for both v- and h-pol channels occur at elapsed times of approximately 200 s. Because this is significantly longer than the ∼30-s minimum shown in Fig. 3, radiometer, not CNCS, instability was the limiting factor in the earlier case. In the event that some other RUT was more stable than the CNCS, 200 s would be the upper bound on the time interval during which a complete calibration test set should be measured.

C. CNCS Active-Cold-Load Calibration

The brightness temperature of the CNCS active cold loads was determined by using ambient and LN_2 coaxial reference

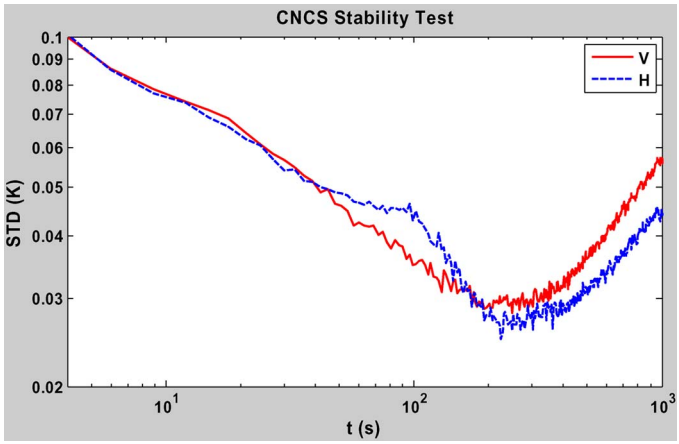

Fig. 4. Allan standard deviation versus integration time of frequently recalibrated radiometer measurements while viewing the CNCS AWG signal characterizes the inherent stability of the CNCS signal source.

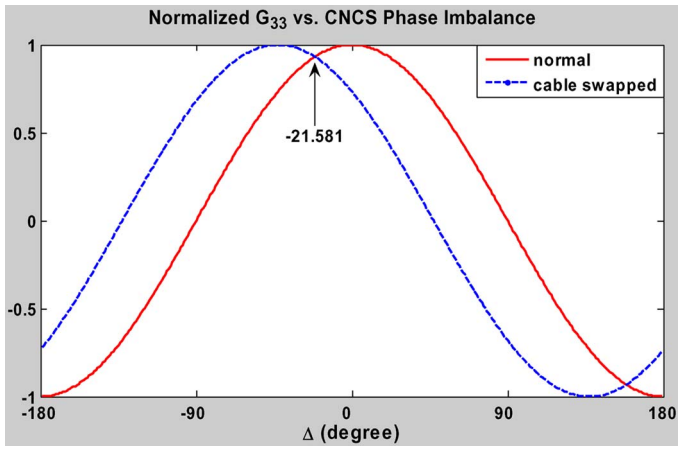

Fig. 5. CNCS channel phase imbalance Δ is retrieved by swapping v- and h-pol interconnecting cables between the CNCS and RUT. Only one unambiguous value of Δ produces the same estimate of the radiometer gain matrix element G_{33} for both swapped positions.

loads. The LN_2 load- and temperature-regulated coaxial cable is a precision Maury Microwave MT7118 system with ± 0.5-K uncertainty. Measurement of the LN_2 and ambient loads provides an absolute calibration of the RUT. Subsequent measurement of the active load allows the calibration to be transferred to the active cold load. The brightness temperatures of the active cold loads are found in this way to be 87.6 and 92.3 K for the v- and h-pol channels, respectively, without correction for impedance mismatches and 85.5 and 90.0 K with the corrections applied. This procedure has been repeated numerous times over periods of weeks and months and found to be repeatable at approximately the 1-K level. It should be noted that the brightness temperature of the active cold load should be recalibrated if a different RUT is used or if the passband characteristics of a RUT change significantly. This is because the brightness temperature of the reverse LNA at the heart of the active cold load is more frequency-dependent than is a traditional LN_2 load, and so, the effective brightness temperature of the active cold load will be more dependent on the specific passband frequency response of a radiometer.

D. CNCS Cable Cross-Swapping for Channel Phase Imbalance

The CNCS channel phase imbalance Δ is determined by manually cross-swapping the interconnecting cables between the CNCS and the RUT. When cross-swapped, CNCS output port V is connected to radiometer input channel H, and CNCS output port H is connected to radiometer input channel V. Cross-swapping changes the sign, but not the magnitude, of Δ in the CNCS forward model. In both the standard and cross-swapped positions, the radiometer parameters that are retrieved should be the same, since the radiometer itself has not changed. Some of the parameters (e.g., G_{vv} and G_{hh}) are not sensitive to either the radiometer or the CNCS channel phase imbalance. Other parameters (e.g., G_{33}) are sensitive to the CNCS channel phase imbalance and, so, will vary depending on what value is assumed for Δ.

E. Retrieving the CNCS Forward-Model Parameters

The Newton–Raphson method is not able to estimate the CNCS channel phase imbalance Δ. It can, however, estimate all other of the CNCS and RUT forward-model parameters if Δ is known. In order to solve for Δ, its assumed value is varied over all possible angles from 0° to 360°, and for each value, all other CNCS and RUT parameters are estimated. This is repeated with both the standard and cross-swapped cable positions. The retrieved values of the RUT parameters should not be affected by the cable arrangement if the correct value for Δ is assumed. If, on the other hand, the wrong value for Δ is used, the retrieval of any phase-sensitive parameters will be affected, and their estimated values will not be the same for both the standard and cross-swapped cable positions. An example of this situation is shown in Fig. 5. The retrieved value of the RUT forward-model parameter G_{33} is shown as a function of the assumed value of Δ in both the standard and cross-swapped cable positions (in the figure, G_{33} has been normalized by $(G_{vv}G_{hh})^{0.5}$ to reduce the effects of radiometer gain fluctuations that may have occurred during the test). There are only two values of Δ for which the same value of G_{33} is retrieved. One of the two values is the correct one, and the other is an ambiguity. The two values differ enough that the ambiguity can be easily resolved by comparing them to an approximate estimate of Δ based on network-analyzer measurements. The correct solution is $\Delta = -21.581^\circ$. The negative value indicates that the electrical length of the v-pol channel is greater than that of the h-pol channel.

Because normalized versions of G_{33} or G_{34} are used to derive the CNCS phase imbalance, cables do not need to be swapped within the time that G_{33} or G_{34} themselves are stable. This is confirmed by the fact that the channel phase imbalance has, in practice, been found to be extremely stable over time.

All other parameters of the CNCS forward model, besides the channel phase imbalance, are retrieved simultaneously with the parameters of the radiometer forward model during the Newton–Raphson process. Those parameters retrieved while the correct value for the CNCS channel phase imbalance is assumed are the correct ones. All parameters of the CNCS forward model are listed in Table II. Monte Carlo simulation

TABLE II
RETRIEVED CNCS-CALIBRATION PARAMETERS

k_v (unitless)	k_h (unitless)	$O_{awg,v}$ (K)	$O_{awg,h}$ (K)	Δ ($^\circ$)
1.0825	0.9798	8.3200	6.8432	-21.581

shows that the precision (i.e., rms uncertainty) of the CNCS output is 0.18 and 0.13 K for the v- and h-pol channels, respectively. The precision of the CNCS channel phase imbalance is assumed to be the same as that of the radiometer phase imbalance, namely, 0.02°.

F. Retrieving the RUT Forward-Model Parameters

The retrieved polarimetric gain matrix and offsets of the RUT [as defined by (4)] are listed in Table III. The rms errors in each parameter, as determined by a Monte Carlo simulation of the retrieval process, are also listed in the table. Once the gain matrix is known, the radiometer channel phase imbalance can be obtained from G_{33} and G_{34} by

$$\Delta\phi = \begin{cases} \sin^{-1}\left(\frac{G_{34}}{\sqrt{G_{33}^2+G_{34}^2}}\right), & if \quad G_{33} \geq 0 \\ 180^0 - \sin^{-1}\left(\frac{G_{34}}{\sqrt{G_{33}^2+G_{34}^2}}\right), & if \quad G_{33} < 0\,. \end{cases} \tag{8}$$

The channel phase imbalance using (8) is 21.39°, with a positive imbalance indicating that the v-pol channel has a longer electrical length. This result was corroborated by a direct measurement of the relative phaselength of the analog portions of the v- and h-pol branches of the radiometer. A sinusoidal test signal was split and fed into the v- and h-pol input ports of the radiometer. The phase difference between them at the output ports of the demodulator was measured as 18.14°. The small discrepancy between this value and that determined using (8) is likely due to the phase imbalance of the 3-dB splitter used to generate the test signal and to the phase imbalances in the digital back end of the radiometer, which were not included in the test using the sinusoidal signal.

V. VALIDATION OF THE RETRIEVED CALIBRATION PARAMETERS

The calibration algorithm estimates both CNCS and RUT forward-model parameters simultaneously. Because both forward models account for nonideal characteristics, several test were performed to ensure that nonidealities in the CNCS did not influence the parameters retrieved for the RUT, and vice versa. The tests involved introducing certain changes into either the CNCS or RUT hardware and, then, verifying that the changes in the retrieved parameters responded accordingly.

A. CNCS Channel Gain Imbalance

A coaxial attenuator was inserted between the AWG and the RF head of the CNCS, first, along the v-pol and, then, along the h-pol signal paths. The attenuation was measured to be 1.91 dB by a network analyzer. The retrieved CNCS channel-gain-imbalance parameters [k_v and k_h in (2)] were altered as a result. Using the new retrieved values for k_v and k_h, the maximum possible brightness temperature that the CNCS could generate decreased by 1.84 and 1.89 dB for the v- and h-pol channels, respectively. The differences from the 1.91-dB change predicted by the network-analyzer measurement likely result from a combination of CNCS parameter-estimation errors, network-analyzer measurement errors, and the differences in impedance matching for each of the three cases.

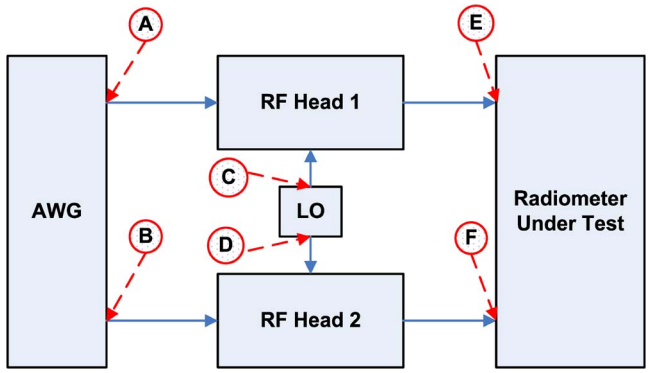

Fig. 6. Locations where an additional adapter was inserted to verify the proper retrieval of phase imbalances between v- and h-pol channels. The circled letters indicate the placement of the adapter.

B. CNCS and Radiometer Channel Phase Imbalances

A subminiature version A (SMA) male/female adapter was inserted at various places along the CNCS coaxial signal path or between the CNCS and the RUT. The adapter introduces an additional phase imbalance into the system. The locations where the adapter was added are shown in Fig. 6. For each position of the adapter, the complete calibration procedure was followed in order to retrieve all forward-model parameters—in particular, both the CNCS and the radiometer channel phase imbalances. One or the other of the phase imbalances (but not both) should change, depending on where the adapter was placed. The retrieved change should be close to the electrical length of the SMA adapter itself, as determined independently by a network analyzer. Small differences are possible due impedance mismatches between the adapter and the circuit at its point of insertion. Results of these tests are summarized in Table IV. In the table, the letter given in column 1 (SMA location) matches the spot shown in Fig. 6 where the SMA adapter was inserted. Column 2 ($\Delta\theta_{\mathrm{CNCS}}$) gives the change in the CNCS phase imbalance Δ due to the insertion of the adapter. Column 3 ($\Delta\theta_{\mathrm{RAD}}$) gives the change in the radiometer phase imbalance, as defined by (8), due to the insertion of the adapter. Column 4 (predicted phase shift) gives the change predicted based on network-analyzer measurements, which varies with each adapter location, because the frequency of the signal changes. Column 5 (retrieval error) gives the difference between the predicted and retrieved change in phase imbalance for the retrieved imbalance that was supposed to change. The change in the other imbalance should, in all cases, have been zero.

TABLE III
RETRIEVED RADIOMETER POLARIMETRIC GAIN MATRIX AND OFFSET VECTOR

G_{xy} (Counts/K) and O_x (Counts)		*Input*				
		v-pol (Counts/K)	*h-pol* (Counts/K)	*3rd Stokes* (Counts/K)	*4th Stokes* (Counts/K)	*Offset* (Counts)
Output	*v-pol*	12.950 ± 0.01	-0.003 ± 0.01	0.0094 ± 0.004	0.0003 ± 0.004	3515.19 ± 0.5
	h-pol	-0.0011 ± 0.008	11.7785 ± 0.008	0.0040 ± 0.003	-0.0260 ± 0.003	3925.08 ± 0.4
	3rd Stokes	0.0068 ± 0.003	0.0096 ± 0.003	5.7920 ± 0.003	2.2690 ± 0.002	-31.81 ± 0.3

The sign of the changes in phase imbalance listed in Table IV follows sign conventions for the imbalance in the v-pol channel relative to the h-pol channel. In each case, the phase shift due to the adapter has the predicted sign. The rms error in magnitude of the retrieved phase shift over all six cases, relative to the value predicted by the network-analyzer measurements of the adapter, is 0.8°. Any change in the retrieved phase imbalance for the portion of the system that was not affected by the insertion of the adapter represents an error. These are the shaded entries in Table IV. The rms value of these errors, over all six cases, is 0.3°.

TABLE IV
VERIFICATION OF CHANNEL PHASE IMBALANCE RETRIEVAL

SMA adapter Location	$\Delta\theta_{CNCS}$* (deg)	$\Delta\theta_{RAD}$** (deg)	Predicted Phase Shift (deg)	Retrieval Error (deg)
A	-7.005	0.141	-7.20	0.195
B	8.018	0.258	7.20	0.818
C	-23.554	-0.008	-24.33	0.776
D	24.677	0.204	24.33	0.347
E	0.205	-32.581	-31.55	-1.031
F	0.620	32.833	31.55	1.283

*$\Delta\theta_{CNCS}$ is the CNCS phase imbalance shift due to the SMA adapter

**$\Delta\theta_{RAD}$ is the radiometer phase imbalance shift due to the SMA adapter

VI. CONCLUSION

Test procedures and data-analysis algorithms have been presented to calibrate a fully polarimetric-radiometer receiver using the CNCS. The CNCS is a digital microwave-signal generator capable of producing pairs of simulated thermal noise signals which have independent programmable brightness temperatures and partial correlation. In order to accurately calibrate the radiometer, it is necessary to identify and quantify the nonideal characteristics of the CNCS. In other words, the calibration source must also be calibrated. It is possible to calibrate both the radiometer and CNCS simultaneously, provided that a sufficient number and variety of test signals and conditions are generated.

Simultaneous calibration is approached by developing parameterized forward models for both the CNCS and radiometer. The CNCS forward model describes the relationship between the digitally programmable settings of the signal generator and the actual brightness temperatures that are generated. The radiometer forward model, in turn, describes the relationship between the brightness temperatures entering its input ports and the detector counts recorded on its data system. Composed together, the complete forward model relates programmable CNCS settings to radiometer counts. The simultaneous calibration algorithm estimates the parameters of the complete forward model from the counts that are measured, while the CNCS settings are varied over a suitable range.

The calibration method has been demonstrated using L-band versions of the CNCS and a correlating polarimetric radiometer. All elements of the polarimetric gain matrix of the radiometer are solved for, including the off-diagonal elements that account for gain and phase imbalances between polarimetric channels. All necessary gain and phase imbalance parameters of the CNCS are also retrieved. The validity of the solutions is tested by intentionally modifying the amplitude and phase imbalances of both the CNCS and the radiometer in known ways and, then, verifying that the calibration procedure correctly identifies the changes. In all cases, the tests were successful. In particular, the calibration procedure was correctly able to identify whether a change was made to the CNCS or the radiometer and whether the change altered the amplitude or the phase imbalance between v- and h-pol channels.

The CNCS has both advantages and limitations relative to other methods for calibrating a polarimetric radiometer. The most important limitation is the fact that, because it is installed in place of a radiometer's antenna, the CNCS cannot calibrate the effects of the antenna itself on measurement of the Stokes parameters in brightness temperature. Cross-pol leakage in the

antenna, for example, would not be accounted for by the off-diagonal terms of the polarimetric gain matrix estimated by the CNCS. Those terms would only characterize the behavior of the receiver, orthomode transducer, and other components and subsystems present during CNCS testing. Antenna effects would still need to be accounted for by some other means—typically with antenna-range measurements and/or on-orbit intercomparisons with groundtruth-based radiative-transfer model predictions. Other, relatively minor, limitations with a CNCS calibration include the available bandwidth of its simulated noise (currently limited to 500 MHz by the clock rate of the commercial AWG being used) and the fact that the effective brightness temperature generated by the CNCS needs to be recalibrated whenever changes are made to the radiometer passband response (because the CNCS active cold load has a frequency-dependent brightness temperature).

The primary advantages of CNCS calibration are its simplicity and automation and its flexibility. The ready availability of a variable brightness-temperature source during receiver development, integration, and testing, without the need for LN_2 cooling, can be extremely convenient and time saving. The ability to generate known third and fourth Stokes parameters in brightness temperature, to vary them in a known way, and to be able to precisely and accurately reproduce them later can greatly simplify the characterization and trouble shooting of a polarimetric receiver during its development phase. Moreover, the fact that variations in both signal strength and polarization coherence are programmable makes fully automated testing straightforward. The precision, or repeatability, of estimates of the polarimetric gain matrix and offset vector was shown to be approximately 0.2 K for the gain elements and 0.05 K for the offsets. The accuracy of the retrieved CNCS-calibration parameters can be estimated by comparisons with network-analyzer measurements of the radiometer components. The phase imbalance between v- and h-pol channels, introduced by adding an SMA adapter (see Section IV-B), was estimated with 0.8° accuracy. Changes in amplitude of the CNCS channels are more difficult to validate due to the inherent inaccuracies associated with the network-analyzer measurements of absolute component losses. CNCS amplitudes have been validated with an accuracy of, at best, several kelvins.

Absolute end-to-end calibration of any radiometer is best done with the complete system, including its antenna, assembled while viewing external calibration targets. The greatest value of the CNCS is as a tool during radiometer development. It can generate precise and repeatable variations in the full Stokes parameters in brightness temperature. This permits a determination of the relative response of the radiometer to known changes in its input.

APPENDIX
CORRECTION FOR IMPEDANCE MISMATCHES AT THE RADIOMETER INPUT PORT

A model for impedance mismatches between a radiometer receiver and its antenna has been developed by Corbella *et al.* [17], [18]. Their approach is adopted in this paper. The brightness temperature of the CNCS active cold load is determined by a two-point calibration using an ambient-temperature coaxial termination and one immersed in LN_2. The digital counts measured by the RUT while connected to each of the LN_2 reference load, ambient reference load, and CNCS active cold load are, respectively, given by

$$C_{\mathrm{LN2}} = g\left\{|\Lambda_{\mathrm{LN2}}|^2 T_{\mathrm{LN2}} + |\Lambda_{\mathrm{LN2}}|^2 |\Gamma_{\mathrm{LN2}}|^2 T_r + 2\mathrm{Re}[\Lambda_{\mathrm{LN2}}\Gamma_{\mathrm{LN2}} T_c] + T_R\right\} \tag{A1}$$

$$C_{\mathrm{ref}} = g\left\{|\Lambda_{\mathrm{CNCS}}|^2 T_{\mathrm{ref}} + |\Lambda_{\mathrm{CNCS}}|^2 |\Gamma_{\mathrm{CNCS}}|^2 T_r + 2\mathrm{Re}[\Lambda_{\mathrm{CNCS}}\Gamma_{\mathrm{CNCS}} T_c] + T_R\right\} \tag{A2}$$

$$C_{\mathrm{Cold}} = g\left\{|\Lambda_{\mathrm{CNCS}}|^2 T_{\mathrm{Cold}} + |\Lambda_{\mathrm{CNCS}}|^2 |\Gamma_{\mathrm{CNCS}}|^2 T_r + 2\mathrm{Re}\left[\Lambda_{\mathrm{CNCS}}\Gamma_{\mathrm{CNCS}} T_c\right] + T_R\right\} \tag{A3}$$

where g is the radiometer gain, T_{LN2}, T_{ref}, and T_{Cold} are the brightness temperatures of the LN_2 reference load, ambient reference load, and CNCS active cold load, respectively, that would be measured by a radiometer with a perfect impedance match, Γ_{LN2} and Γ_{CNCS} are the voltage reflection coefficients when viewing the LN_2 reference load and the CNCS active cold load, and $\Lambda_y = (1 - S_{11,\mathrm{rad}}\ \Gamma_y)^{-1}$ (for $y = \mathrm{LN}_2$ and CNCS), where $S_{11,\mathrm{rad}}$ is the input reflection coefficient of the radiometer receiver. In (A1)–(A3), T_r is the noise temperature exiting the receiver toward the antenna, T_R is the traditional receiver noise temperature, and T_c is the component of T_r and T_R that is correlated. For cases of high isolation at the radiometer input port, T_c is given by [17]

$$T_c = -T_{\mathrm{phy}}\left(S_{11,\mathrm{FE}} + \frac{S_{12,\mathrm{FE}} S^*_{22,\mathrm{FE}}}{S^*_{21,\mathrm{FE}}}\right) \tag{A4}$$

where T_{phy} is the physical temperature of the radiometer front-end components preceding the first gain stage and $S_{xy,\mathrm{FE}}$ for $x, y = 1, 2$ are the S parameters for the radiometer front end (see [17] and [18] for detailed definitions of these noise temperatures). Port 1 for these S parameters is the input to the radiometer, and port 2 is the output from the first gain stage of the receiver (i.e., the point after which internally generated noise ceases to have a significant effect on the overall receiver noise temperature). The fact that the radiometer includes an isolator at its input port with a good ($\sim$25 dB) level of isolation insures that T_r is approximately equal to T_{phy}.

All of the reflection coefficients and other S parameters in (A1)–(A3) can be measured directly using a network analyzer. The warm- and cold-reference brightness temperatures, T_{ref} and T_{LN2}, are also known. The remaining three unknown variables (g, T_R, and T_{Cold}) can be solved algebraically from the three simultaneous equations [(A1)–(A3)]. The value for T_{Cold} determined in this way is the brightness temperature that would be presented by the CNCS active cold load to a radiometer with a perfect impedance match. For the L-band CNCS, T_{Cold} is found to be approximately 2 K lower than its value would have been had the effects of impedance mismatches been ignored. The actual T_{Cold} that would be measured by a

particular radiometer will depend on the impedance match of its input port.

The effect on the measured Stokes parameters in brightness temperature of impedance mismatches between a radiometer's antenna and its receiver, and of crosstalk between the orthogonal polarimetric channels of a radiometer's antenna, has also been considered previously by Corbella *et al.* [17]. Their approach is again adopted here, replacing the antenna by the CNCS and using the impedance mismatch and isolation characteristics of the CNCS. The modified Stokes parameters are related to the true values by (A5), shown at the bottom of the page, where T_y' are the modified brightness temperatures and T_y are the values that would have been measured if the impedance match was perfect and there was no polarization crosstalk $(y = v, h, 3,$ and $4)$, S_{xy} $(x, y = v, h)$ are the S parameters of the CNCS, $S_{11,\mathrm{rad},x}$ $(x = v, h)$ is the reflection coefficient at the input ports of the RUT, and the subscripts v and h denote the v- and h-pol channels of the CNCS and RUT. The offset brightness temperatures, $T_{ex,y}$ $(y = v, h, 3,$ and $4)$ are defined by

$$T_{ex,v} = |S_{vv}|^2 T_{r,v} + |S_{vh}|^2 T_{r,h} + 2\mathrm{Re}\{S_{vv} T_{c,v}\} \quad \text{(A6.1)}$$

$$T_{ex,h} = |S_{hh}|^2 T_{r,h} + |S_{hv}|^2 T_{r,v} + 2\mathrm{Re}\{S_{hh} T_{c,h}\} \quad \text{(A6.2)}$$

$$T_{ex,3} = 2\mathrm{Re}\{S_{vv} S_{hv}^* T_{r,v} + S_{vh} S_{hh}^* T_{r,h} + S_{hv}^* T_{c,v}^* + S_{vh} T_{c,h}\} \quad \text{(A6.3)}$$

$$T_{ex,4} = 2\mathrm{Im}\{S_{vv} S_{hv}^* T_{r,v} + S_{vh} S_{hh}^* T_{r,h} + S_{hv}^* T_{c,v}^* + S_{vh} T_{c,h}\} \quad \text{(A6.4)}$$

(see [17] for detailed descriptions of these correction algorithms).

The corrections to the Stokes parameters given by (A5) and (A6) can be incorporated directly into the elements of the polarimetric gain matrix and offset vectors. Define G and O as the gain matrix and offset vector of the RUT prior to correction, and G' and O' as the same after correction. Using (A5), they are related by (A7), shown at the top of the page. Solving for the corrected values, G' and O', gives (A8), shown at the top of the page.

Equation (A8) is the general expression for corrections to the gain matrix and offset vector. A simplified special case applies for the CNCS, because the isolation between its v- and h-pol channels is extremely high (∼75 dB). In this case, S_{hv} and S_{vh} can be assumed equal to zero. The corrections given in (A8) then simplify to

$$[G'|O'] = [G|O] \cdot \begin{bmatrix} 1 & 0 & 0 & 0 & -|S_{vv}|^2 T_{r,v} - 2\mathrm{Re}\{S_{vv} T_{c,v}\} \\ 0 & 1 & 0 & 0 & -|S_{hh}|^2 T_{r,h} - 2\mathrm{Re}\{S_{hh} T_{c,h}\} \\ 0 & 0 & 1 & 0 & 0 \\ 0 & 0 & 0 & 1 & 0 \\ 0 & 0 & 0 & 0 & 1 \end{bmatrix}. \quad \text{(A9)}$$

Equation (A9) demonstrates that the RUT polarimetric gain matrix is unaffected by impedance mismatches, provided that isolation between the v- and h-pol channels is high. Only the offset vector is affected. Note that the gain matrix and offset

$$\begin{bmatrix} T_v' \\ T_h' \\ T_3' \\ T_4' \end{bmatrix} = \begin{bmatrix} 1 & 0 & 0 & 0 & T_{ex,v} \\ 0 & 1 & 0 & 0 & T_{ex,h} \\ 2\mathrm{Re}\left\{S_{hv}^* S_{11,\mathrm{rad},v}^*\right\} & 2\mathrm{Re}\{S_{vh} S_{11,\mathrm{rad},h}\} & 1 & 0 & T_{ex,3} \\ 2\mathrm{Im}\left\{S_{hv}^* S_{11,\mathrm{rad},v}^*\right\} & 2\mathrm{Im}\{S_{vh} S_{11,\mathrm{rad},h}\} & 0 & 1 & T_{ex,4} \end{bmatrix} \cdot \begin{bmatrix} T_v \\ T_h \\ T_3 \\ T_4 \\ 1 \end{bmatrix} \quad \text{(A5)}$$

$$[G|O] = [G'|O'] \cdot \begin{bmatrix} 1 & 0 & 0 & 0 & T_{ex,v} \\ 0 & 1 & 0 & 0 & T_{ex,h} \\ 2\mathrm{Re}\left\{S_{hv}^* S_{11,\mathrm{rad},v}^*\right\} & 2\mathrm{Re}\{S_{vh} S_{11,\mathrm{rad},h}\} & 1 & 0 & T_{ex,3} \\ 2\mathrm{Im}\left\{S_{hv}^* S_{11,\mathrm{rad},v}^*\right\} & 2\mathrm{Im}\{S_{vh} S_{11,\mathrm{rad},h}\} & 0 & 1 & T_{ex,4} \\ 0 & 0 & 0 & 0 & 1 \end{bmatrix} \quad \text{(A7)}$$

$$[G'|O'] = [G|O] \cdot \begin{bmatrix} 1 & 0 & 0 & 0 & T_{ex,v} \\ 0 & 1 & 0 & 0 & T_{ex,h} \\ 2\mathrm{Re}\left\{S_{hv}^* S_{11,\mathrm{rad},v}^*\right\} & 2\mathrm{Re}\{S_{vh} S_{11,\mathrm{rad},h}\} & 1 & 0 & T_{ex,3} \\ 2\mathrm{Im}\left\{S_{hv}^* S_{11,\mathrm{rad},v}^*\right\} & 2\mathrm{Im}\{S_{vh} S_{11,\mathrm{rad},h}\} & 0 & 1 & T_{ex,4} \\ 0 & 0 & 0 & 0 & 1 \end{bmatrix}^{-1} \quad \text{(A8)}$$

vector would need to be corrected again using the impedance and crosstalk characteristics of the antenna when it is attached to the RUT instead.

REFERENCES

[1] L. Tsang, J. A. Kong, and R. T. Shin, *Theory of Microwave Remote Sensing*. New York: Wiley, 1985.

[2] S. H. Yueh, R. Kwok, F. K. Li, S. V. Nghiem, and W. J. Wilson, "Polarimetric passive remote sensing of ocean wind vectors," *Radio Sci.*, vol. 29, no. 4, pp. 799–814, Jul. 1994.

[3] S. H. Yueh, "Estimates of Faraday rotation with passive microwave polarimetry for microwave remote sensing of Earth surfaces," *IEEE Trans. Geosci. Remote Sens.*, vol. 38, no. 5, pp. 2434–2438, Sep. 2000.

[4] C. S. Ruf, "Constraints on the polarization purity of a Stokes microwave radiometer," *Radio Sci.*, vol. 33, no. 6, pp. 1617–1639, 1998.

[5] A. Ishimaru, *Electromagnetic Wave Propagation, Radiation, and Scattering*. Englewood Cliffs, NJ: Prentice-Hall, 1991.

[6] J. R. Piepmeier, "Calibration of passive microwave polarimeters that use hybrid coupler-based correlators," *IEEE Trans. Geosci. Remote Sens.*, vol. 42, no. 2, pp. 391–400, Feb. 2004.

[7] S. H. Yueh, W. J. Wilson, F. K. Li, S. V. Nghiem, and W. B. Ricketts, "Polarimetric brightness temperatures of sea surfaces measured with aircraft K- and Ka-band radiometers," *IEEE Trans. Geosci. Remote Sens.*, vol. 35, no. 5, pp. 1177–1187, Sep. 1997.

[8] O. A. Peverini, R. Tascone, E. Carretti, G. Virone, A. Olivieri, R. Orta, S. Cortiglioni, and J. Monari, "On-board calibration system for millimeter-wave radiometers based on reference-polarized signal injection," *IEEE Trans. Microw. Theory Tech.*, vol. 54, no. 1, pp. 412–420, Jan. 2006.

[9] A. J. Gasiewski and D. B. Kunkee, "Calibration and applications of polarization-correlating radiometers," *IEEE Trans. Microw. Theory Tech.*, vol. 41, no. 5, pp. 767–773, May 1993.

[10] J. Lahtinen and M. T. Hallikainen, "HUT fully polarimetric calibration standard for microwave radiometry," *IEEE Trans. Geosci. Remote Sens.*, vol. 41, no. 3, pp. 603–611, Mar. 2003.

[11] C. S. Ruf and J. Li, "A correlated noise calibration standard for interferometric, polarimetric, and autocorrelation microwave radiometers," *IEEE Trans. Geosci. Remote Sens.*, vol. 41, no. 10, pp. 2187–2196, Oct. 2003.

[12] C. S. Ruf and J. Li, "Evaluation of correlation radiometers using programmable correlated noise," in *Proc. 2nd Int. Microw. Radiometer Calibration Workshop*, Barcelona, Spain, 2002.

[13] D. M. Le Vine, G. S. E. Lagerloef, F. R. Colomb, S. H. Yueh, and F. A. Pellerano, "Aquarius: An instrument to monitor sea surface salinity from space," *IEEE Trans. Geosci. Remote Sens.*, vol. 45, no. 7, pp. 2040–2050, Jul. 2007.

[14] J. Peng, C. Ruf, S. Brown, and J. Piepmeier, "Characterization of the Aquarius and Juno radiometers using a programmable digital noise source," in *Proc. IGARSS*, Barcelona, Spain, 2007, pp. 2416–2418.

[15] S. H. Yueh, R. West, W. J. Wilson, F. K. Li, E. G. Njoku, and Y. Rahmat-Samii, "Error sources and feasibility for microwave remote sensing of ocean surface salinity," *IEEE Trans. Geosci. Remote Sens.*, vol. 39, no. 5, pp. 1049–1060, May 2001.

[16] C. S. Ruf, S. M. Gross, and S. Misra, "RFI detection and mitigation for microwave radiometry with an agile digital detector," *IEEE Trans. Geosci. Remote Sens.*, vol. 44, no. 3, pp. 694–706, Mar. 2006.

[17] I. Corbella, F. Torres, A. Camps, N. Duffo, M. Vall-llossera, K. Rautiainen, M. Martin-Neira, and A. Colliander, "Analysis of correlation and total power radiometer front-ends using noise waves," *IEEE Trans. Geosci. Remote Sens.*, vol. 43, no. 11, pp. 2452–2459, Nov. 2005.

[18] I. Corbella, A. Camps, F. Torres, and J. Bara, "Analysis of noise-injection networks for interferometric-radiometer calibration," *IEEE Trans. Microw. Theory Tech.*, vol. 48, no. 4, pp. 545–552, Apr. 2000.

[19] R. Schieder, G. Rau, and B. Vowinkel, "Characterization and measurement of radiometer stability," in *Proc. 14th Eur. Microw. Conf.*, 1984, pp. 248–253.

[20] J. Lahtinen, A. J. Gasiewski, M. Klein, and I. Corbella, "A calibration method for fully polarimetric microwave radiometers," *IEEE Trans. Geosci. Remote Sens.*, vol. 41, no. 3, pp. 588–602, Mar. 2003.

Jinzheng Peng (S'06–M'08) received the B.S. degree in electrical engineering from Wuhan University, Wuhan, China, in 1991 and the M.S. degree in electrical engineering from the University of Massachusetts, Amherst, in 2003. He is currently working toward the Ph.D. degree with the Remote Sensing Group at the Space Physics Research Laboratory, University of Michigan, Ann Arbor.

He was with the Beijing Institute of Remote Sensing Equipment, Beijing, China, from 1991 to 2000. His research interests include system-level concept development and design, analysis, and calibration for microwave remote-sensing instruments.

Christopher S. Ruf (S'85–M'87–SM'92–F'01) received the B.A. degree in physics from Reed College, Portland, OR, and the Ph.D. degree in electrical and computer engineering from the University of Massachusetts, Amherst.

He was with Intel Corporation, Hughes Space and Communication, the NASA Jet Propulsion Laboratory, and Penn State University. In 2000, he was a Guest Professor with the Technical University of Denmark, Lyngby, Denmark. He is currently a Professor of atmospheric, oceanic, and space sciences and electrical engineering and computer science and the Director with the Space Physics Research Laboratory, University of Michigan, Ann Arbor. He has published in the areas of microwave radiometer satellite calibration, sensor and technology development, and geophysical retrieval algorithms.

Dr. Ruf is a member of the American Geophysical Union (AGU), American Meteorological Society (AMS), and Commission F of the Union Radio Scientifique Internationale. He has served or is serving on the Editorial Boards of the IEEE GRS-S NEWSLETTER, the *AGU Radio Science*, the IEEE TRANSACTIONS ON GEOSCIENCE AND REMOTE SENSING, and the *AMS Journal of Atmospheric and Oceanic Technology*. He was the recipient of three NASA Certificates of Recognition and four NASA Group Achievement Awards, as well as the 1997 GRS-S Transactions Prize Paper Award, the 1999 IEEE Judith A. Resnik Technical Field Award, and the IGARSS 2006 Symposium Prize Paper Award.